dc Josephson Effect in Altermagnets

Jabir Ali Ouassou, Arne Brataas, and Jacob Linder
Center for Quantum Spintronics, Department of Physics, Norwegian University of Science and Technology, NO-7491 Trondheim, Norway

(Received 11 January 2023; revised 1 April 2023; accepted 11 July 2023; published 17 August 2023)

The ability of magnetic materials to modify superconductors is an active research area for possible applications in thermoelectricity, quantum sensing, and spintronics. We consider the fundamental properties of the Josephson effect in a class of magnetic materials that recently have attracted much attention: altermagnets. We show that despite having no net magnetization and a band structure qualitatively different from ferromagnets and from conventional antiferromagnets without spin-split bands, altermagnets induce 0-π oscillations. The decay length and oscillation period of the Josephson coupling are qualitatively different from ferromagnetic junctions and depend on the crystallographic orientation of the altermagnet. The Josephson effect in altermagnets thus serves a dual purpose: it acts as a signature that distinguishes altermagnetism from ferromagnetism and conventional antiferromagnetism and offers a way to control the supercurrent via flow direction anisotropy.

DOI: 10.1103/PhysRevLett.131.076003

Introduction.—Spin splitting of quasiparticle bands is a crucial material property for spintronics [1]. Recent works have predicted such splitting, and related effects, distinct from ferromagnetic and relativistically spin-orbit coupled systems [2–5]. Reference [6] envisioned non-relativistic momentum-dependent spin splitting due to a spatially varying magnetic field, albeit in a different context than compensated magnetic systems. Instead, Refs. [2–5] considered spin-compensated magnetic systems and demonstrated the possibility of a huge momentum-dependent spin splitting even in collinearly ordered antiferromagnets. In both cases, spin splitting occurs even without atomic spin-orbit coupling—and can be significantly stronger due to their nonrelativistic origin. Materials with this type of band structure have been dubbed *altermagnets* [7,8] due to the alternating $d/g/i$-wave spin order in their electronic structure. Magnetic octupoles [9] may be a suitable order parameter for altermagnets. They have a large $\boldsymbol{k}$-dependent spin splitting of the bands, which is even in powers of $\boldsymbol{k}$. *Ab initio* calculations identified several potential altermagnets, including metals like RuO_2 and Mn_5Si_3 and semiconductors or insulators like MnF_2 and La_2CuO_4 [4,5,8,10–13]. High-quality monodomain crystals are central to realizing the altermagnetic band structure.

Through the proximity effect, nonsuperconducting metals can inherit the two fundamental characteristics of superconductors: the Meissner effect [14] and dissipationless charge flow [15]. When magnets become superconducting via the proximity effect, both the Meissner effect and dissipationless transport change in qualitatively new ways. For instance, the Josephson coupling through ferromagnets displays 0-π oscillations [16,17]: The ground-state phase difference between the superconductors alternates between 0 and π, depending on junction parameters. As a result, the supercurrent vanishes at certain lengths and temperatures. So-called π junctions can be used for qubits [18,19], and have also been generalized to ϕ_0 junctions

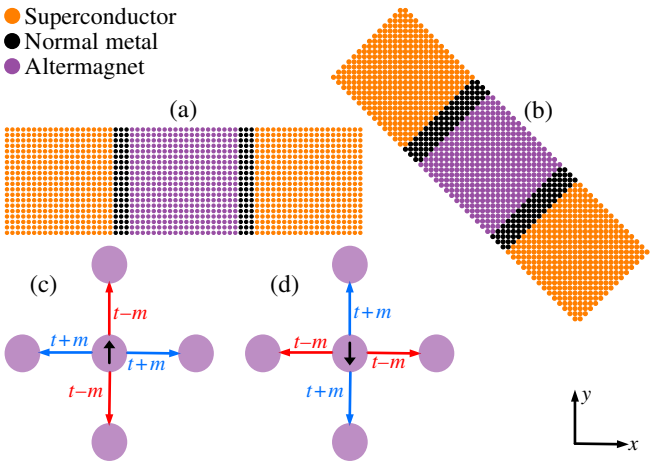

FIG. 1. (a)–(b) Josephson junctions considered here. Each circle represents one atom in a 2D square lattice in real space. Experimentally, there is likely a lattice mismatch between the different regions at the interfaces, which can reduce the supercurrent. The unit vectors $\boldsymbol{n}$, $\boldsymbol{e}_x$, $\boldsymbol{e}_y$ point along the interface normals, x axis, and y axis, respectively. (a) "Straight junctions" are aligned with the crystallographic axes, thus $\boldsymbol{n} = \boldsymbol{e}_x$. (b) "Diagonal junctions" have 45° misalignment relative to the lattice, so $\boldsymbol{n} = (\boldsymbol{e}_x - \boldsymbol{e}_y)/\sqrt{2}$. (c)–(d) Illustration of the altermagnetic order parameter $\boldsymbol{m}_{ij}$. (c) Spin-up electrons have increased hopping amplitudes $t \to t + m$ along the x axis, and decreased hopping amplitudes $t \to t - m$ along the y axis. (d) For spin-down electrons, the situation is exactly reversed.

[20–22] where the system acts as a quantum phase battery supplying an arbitrary phase $\phi_0 \in (0, \pi)$.

We here consider Josephson junctions with altermagnetic interlayers (see Fig. 1). Surprisingly, we find that despite the absence of any magnetization in altermagnets, the supercurrent displays 0-π oscillations. The behavior is different from both ferromagnetic and antiferromagnetic Josephson junctions. In antiferromagnets, the π state may occur only in the very specific case of a junction with exactly an odd number of atoms [23,24], so that a net magnetic moment exists. In addition, we find that both the decay and oscillation period of the supercurrent in the altermagnetic case exhibits anisotropy with respect to the crystallographic orientation of the interface relative the superconductors. The combination of these unique characteristics of the Josephson current in altermagnets distinguishes it from ferromagnets and antiferromagnets and can be used as a tool to identify altermagnets among the list of candidate materials that have recently been identified through *ab initio* calculations [8].

Model.—As shown in Fig. 1, we consider two kinds of Josephson junctions. Both are created from a 2D square lattice with lattice constant a, but have different junction orientations relative to the crystallographic axes. At the ends of each junction is a $20a \times 20a$ BCS superconductor (for diagonal junctions: $14\sqrt{2}a \times 14\sqrt{2}a$). The two superconductors that form each Josephson junction have a variable phase difference $\delta\varphi$. Next to the superconductors are thin normal-metal spacers of lengths $3a$ (straight) or $3\sqrt{2}a$ (diagonal). Finally, the center of each junction is an altermagnet of varying length $L \in [0, 40a]$. All layers are metallic; the current would decrease for insulators.

To model the proposed physical setup we employ the Bogoliubov–de Gennes (BdG) method [25,26]. Our starting point is a mean-field tight-binding Hamiltonian that includes altermagnetism and conventional superconductivity:

$$\mathcal{H} = E_0 - \sum_{i\sigma} \mu_i c^\dagger_{i\sigma} c_{i\sigma} - \sum_i (\Delta_i c^\dagger_{i\downarrow} c^\dagger_{i\uparrow} + \Delta^*_i c_{i\uparrow} c_{i\downarrow}) - \sum_{\langle i,j\rangle\sigma} t_{ij} c^\dagger_{i\sigma} c_{j\sigma} - \sum_{\langle i,j\rangle\sigma\sigma'} (\boldsymbol{m}_{ij} \cdot \boldsymbol{\sigma})_{\sigma\sigma'} c^\dagger_{i\sigma} c_{j\sigma'}, \quad (1)$$

where $c_{i\sigma}$ and $c^\dagger_{i\sigma}$ are the usual electronic annihilation and creation operators, and $\boldsymbol{\sigma} = (\sigma_1, \sigma_2, \sigma_3)$ is the Pauli vector. E_0 describes a constant contribution which is not important for the non-self-consistent calculations below. We choose constant nearest-neighbor hopping amplitudes $t_{ij} \equiv t$ and chemical potentials $\mu_i = -t/2$. In the two superconductors, we set $\Delta_i = \Delta e^{\pm i\delta\varphi/2}$. The gap was calculated using the interpolation formula $\Delta(T) \approx \Delta(0) \tanh[1.74\sqrt{T_c/T - 1}]$, where we chose a zero-temperature gap $\Delta(0) = t/10$. The critical temperature was determined using the BCS ratio $\Delta(0)/T_c \approx 1.764$. The superconducting and altermagnetic terms in Eq. (1) are only present in their respective regions and zero otherwise. In the altermagnet, we set $\boldsymbol{m}_{ij} = +m\boldsymbol{e}_z$ and $\boldsymbol{m}_{ij} = -m\boldsymbol{e}_z$ for hopping along the x and y axes, respectively. This corresponds to a low-energy effective Hamiltonian $mk_xk_y\sigma_z$ or $m(k_x^2 - k_y^2)\sigma_z$ (see Supplemental Material [27]) [4,8], depending on the crystallographic orientation of the sample. This differs from both the momentum-independent spin-splitting $m\sigma_z$ of a ferromagnet and a Rashba spin-orbit coupling $mk_{x(y)}\sigma_z$.

The model above has three parameters that were varied between simulations: The phase difference $\delta\varphi \in \{0, 0.02\pi, \ldots\}$, the altermagnet length $L \in [0, 40a]$, and the magnitude of its order parameter $m \in \{0.05t, 0.15t, 0.50t, 0.90t\}$. While $m \sim 1$ eV is predicted for, e.g., RuO_2 [8], we are unaware of concrete experimental measurements of m, and therefore explore a range of different m values. For each parameter combination, we calculated the Josephson supercurrent I flowing along the junction using the methodology below. The current-phase relation $I(\delta\varphi)$ for each junction was then fit to Fourier sine series, $I(\delta\varphi) = \sum_{n>0} I_n \sin(n\,\delta\varphi)$. The amplitude of the first harmonic I_1 was extracted from these fits, and used to judge whether the Josephson junction is in a 0 state or π state based on its sign. There also exist φ_0 junctions, where also cosine terms must be included in the Fourier expansion; however, we found no sign of φ_0 effects in our simulations. While I_1 is ideal for locating 0-π transitions, we also calculated the critical current $I_c \equiv \max_{\delta\varphi}|I(\delta\varphi)|$ for some interesting junctions as it is more experimentally accessible. Note that $I_c \geq 0$; if, e.g., I_1 and I_2 are important, then $I_c \to |I_2|$ at 0-π transitions since $I_1 \to 0$. For our junctions, I_1 dominates except at 0-π transitions, but higher harmonics could become dominant in shorter junctions at lower temperatures.

Methodology.—The fermionic operators at each site i can be grouped into Nambu vectors $\hat{c}_i \equiv (c_{i\uparrow}, c_{i\downarrow}, c^\dagger_{i\uparrow}, c^\dagger_{i\downarrow})$, which may in turn be collected into a $4N$-element vector $\check{c} \equiv (\hat{c}_1, \ldots, \hat{c}_N)$ containing every fermionic operator on the lattice. The Hamiltonian operator can then be expressed via a $4N \times 4N$ Hamiltonian matrix: $\mathcal{H} = E_0 + \frac{1}{2}\check{c}^\dagger \check{H} \check{c}$. The most common approach to solving the BdG equations consists of diagonalizing $\check{H}$, and then expressing physical observables in terms of its eigenvectors and eigenvalues. However, an alternative approach has gained momentum over the last decade: The Kernel Polynomial Method [28–30]. Instead of diagonalizing the Hamiltonian, one calculates a Green's function matrix from the Hamiltonian matrix, which can be done efficiently and accurately using a series expansion in Chebyshev polynomials.

There are many variants of the Chebyshev methods outlined above. We use the Fermi operator expansion method [31], which for the BdG Hamiltonian is explained in detail in Ref. [32]. The starting point is then the *Fermi matrix* $\check{F} \equiv f(\check{H})$, where $f(\epsilon) = [1 + \exp(\epsilon/T)]^{-1}$ is the Fermi-Dirac distribution at temperature T. The function f should be interpreted in terms of its Taylor expansion when

applied to the matrix $\check{H}$. Using the kernel polynomial method, we can expand the Fermi matrix in Chebyshev polynomials as $\check{F} = \frac{1}{2} f_0 \check{I} + \sum_{m=1}^{M-1} f_m g_m \check{T}_m$, where f_m are the Chebyshev moments of the Fermi-Dirac distribution [28,32], g_m are the Jackson kernel coefficients [28], $\check{T}_m \equiv T_m(\check{H})$ are Chebyshev matrix polynomials [28], and $\check{I}$ is the identity matrix. The above assumes that $\check{H}$ has been normalized such that all eigenvalues have magnitudes below unity; this is in practice easily achieved by scaling $\check{H}$ by its 1-norm. The Chebyshev polynomials are calculated via the usual recursion relation $\check{T}_0 = \check{I}$, $\check{T}_1 = \check{H}$, $\check{T}_m = 2\check{H}\check{T}_{m-1} - \check{T}_{m-2}$ [28]. Calculating $\{\check{T}_m\}$ is the computationally limiting part of our calculation, but was significantly sped up using sparse matrices with fully parallelized blockwise matrix multiplication. All simulations presented here were performed using $M = 4000$ Chebyshev moments. We found that this provides negligible truncation error for typical junctions, consistent with findings for LDOS calculations in Ref. [29]. This procedure yields a $4N \times 4N$ Fermi matrix that can be deconstructed into 4×4 blocks in Nambu space: $\check{F} = [\hat{F}_{ij}]$. Following an approach similar to Ref. [32], one can show that the elements of these matrices are $\hat{F}_{ij} = \langle (\hat{c}_j^\dagger)^{\mathrm{T}} (\hat{c}_i)^{\mathrm{T}} \rangle^{\mathrm{T}}$. Thus, any physical observable that can be calculated from two-point finite-temperature correlation functions on the lattice can be extracted directly from $\check{F}$. Our calculations were performed at a temperature $T = T_c/20$. We evaluate the current in the normal metal as that is computationally simplest. (This is our main motivation for including spacers, which do not significantly affect supercurrents.) Charge conservation ensures that the current is constant anywhere along the junction in a stationary system. We compute the charge current by summing over bond currents. The bond current between two sites i and j can be written [25]

$$J_{ij} = ie \sum_{\sigma} (t_{ij} \langle c_{i\sigma}^\dagger c_{j\sigma} \rangle - t_{ji} \langle c_{j\sigma}^\dagger c_{i\sigma} \rangle), \tag{2}$$

where $e < 0$ is the electron charge. The bond current J_{ij} can be trivially calculated from appropriate traces of $\hat{F}_{ij}$ and $\hat{F}_{ji}$. The bond current along the junction direction $\boldsymbol{n}$ is then simply $J_{ij}(\boldsymbol{\delta}_{ij} \cdot \boldsymbol{n})$, where $\boldsymbol{\delta}_{ij}$ is a unit vector that points from site i towards site j. The total current I flowing through the junction is found by integrating this over a cross section of the junction.

Results and discussion.—The main results of our numerical simulations are in Fig. 2. First, we observe that 0-π oscillations are possible in *both* straight and diagonal junctions. This finding is interesting since such oscillations are typically found in Josephson junctions with *magnetic* interlayers or fine-tuned conventional antiferromagnets with exactly an odd number of atoms, both cases featuring

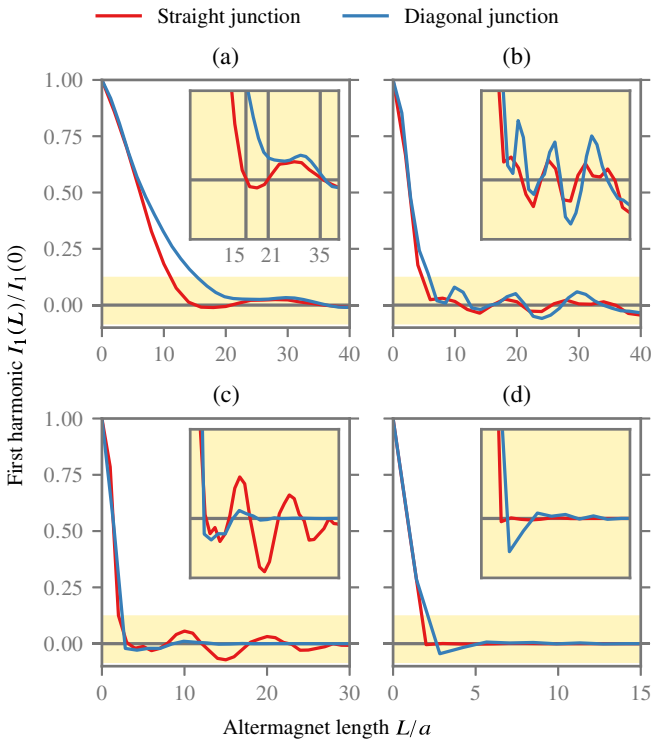

FIG. 2. First harmonic I_1 of the Josephson supercurrent $I(\delta\varphi)$ as function of the altermagnet length L for the junctions in Fig. 1. The net magnetization is zero in all cases. To simplify the comparison between the two different geometries, each curve was normalized to the amplitude $I_1(0)$ in the absence of the altermagnetic interlayer. As indicated above the plots, different panels and curves correspond to different altermagnetic order parameters and junction types, respectively. The insets zoom in on the regions in the golden boxes, in order to highlight the 0-π oscillations for large junction lengths. (a) $m = 0.05t$, (b) $m = 0.15t$, (c) $m = 0.50t$, and (d) $m = 0.90t$.

a net magnetization. In contrast, altermagnets have zero magnetization. Moreover, 0-π oscillations do not appear in Rashba spin-orbit coupled junctions either, which have a different spin-momentum coupling (odd-in-momentum) compared to altermagnets. Second, we see that the 0-π oscillations behave qualitatively differently from ferromagnetic Josephson junctions: the latter typically has an exponential decay with superimposed oscillations [17,33,34], whereas in the altermagnet case there is an initial large decay followed by oscillations with a much weaker damping. This result is most striking in Fig. 2(b), where we find a pure decay at $L < 8a$ followed by nearly pure oscillation at $L > 10a$.

Physically, the oscillations in straight junctions can be understood as follows. Conventional superconductivity consists of singlet Cooper pairs $|\uparrow\downarrow\rangle - |\downarrow\uparrow\rangle$. As the Cooper pairs leak into the altermagnet along the x axis, spin-up electrons have a hopping amplitude $t + m$ while spin-down electrons have a hopping amplitude $t - m$ (see Fig. 1). This "speed difference" causes position-dependent

phase differences between spin-up and spin-down electrons. Such spin-dependent phase shifts are well known to cause 0-π oscillations from previous studies on ferromagnetic Josephson junctions [17,33,34]. For diagonal junctions, however, the most direct path between the superconductors consists of an equal number of hops along the x and y axes. Since the electrons experience opposite spin-dependent phase shifts in these two cases, their effects would be suppressed. However, for other trajectories through the altermagnet, a net spin-dependent phase shift still exists since the number of hops along the x and y axes are different. Overall, the supercurrent oscillations are still present in the diagonal case, but with a longer periodicity as function of junction length. The 0-π oscillations are a robust feature of altermagnetic Josephson junctions, which despite being antiferromagnets have a lifted spin degeneracy of the bands corresponding to a d-wave symmetry and do not require the extreme fine-tuning needed to see 0-π oscillations in conventional antiferromagnets [23].

Figure 2 shows that the initial decay in $I_1(L)$ accelerates as m increases. However, 0-π oscillations are found over a much wider parameter range for straight than diagonal junctions, consistent with the discussion above. For example, for small altermagnetic order parameters $m = 0.05t$ [Fig. 2(a)], the first 0-π oscillation occurs already at $L = 15a$ for the straight junction, but not until $L = 35a$ for the diagonal junction. On the other hand, for large values $m = 0.50t$ [Fig. 2(c)], the first 0-π oscillation occurs simultaneously, but sustained 0-π oscillations for a large range of junction lengths is found only for straight junctions. Qualitatively similar results for straight and diagonal junctions are only found for intermediate values $m = 0.15t$ [Fig. 2(b)]. For very large values $m = 0.90t$, the supercurrent decays extremely fast, limiting the number of visible oscillations for both junction types.

The 0-π oscillation is robust toward small changes in the width W of the junction. In Fig. 3, we plot the first harmonic of the supercurrent vs length L for different W. In straight junctions, the 0-π oscillations are not affected qualitatively by the width of the junctions since the width does not strongly affect the phases the electrons acquire traversing the junctions. In diagonal junctions, wider junctions as compared to the length of the junction imply more possible electron paths straight up-down in Fig. 1(b) so that the physics more resembles that of straight junctions. This is consistent with Fig. 3, where it is seen that when W is lowered the first 0-π oscillations vanish.

To understand the behavior of the supercurrent when the altermagnetic interaction increases, we note that as $m \to t$, spin-down electrons become nearly immobile along the x axis. In this limit, spin-zero Cooper pairs clearly cannot propagate through the altermagnet, and the Josephson effect vanishes. This explains the extremely sharp decay in Fig. 2(d). Interestingly, if an altermagnet with $m \to t$ could be realized experimentally, this might also serve as a new kind of filter for spin-triplet Cooper pairs. Specifically, we would expect $|\uparrow\uparrow\rangle$ pairs to only move along the x axis, $|\downarrow\downarrow\rangle$ pairs to only move along the y axis, and any $|\uparrow\downarrow\rangle \mp |\downarrow\uparrow\rangle$ pairs to decay. This may thus provide a nondestructive way to separate the different equal-spin-triplet pairs generated in superconducting spintronics while eliminating any remaining spin-zero pairs.

In Fig. 4, we show the critical current, rather than just the first harmonic, for one junction ($m = 0.05t$). Measuring $I_c(L)$ experimentally requires precise control over L, as in ferromagnetic Josephson junctions [33]. In Fig. 2(a) we saw that this m yields 0-π oscillations at $L = 15a$ and $L = 21a$ for straight but not diagonal junctions, causing significant I_c suppression. However, due to the presence of higher harmonics, it is difficult from the I_c curve alone in Fig. 4 to observe that there are two 0-π oscillations in this area. We also see that both junctions display a 0-π

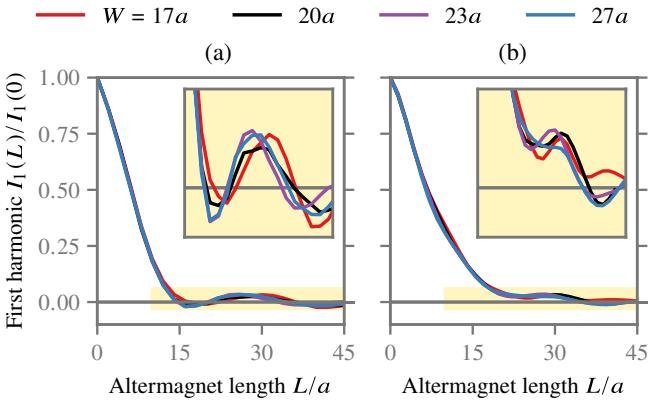

FIG. 3. First harmonic I_1 of the Josephson supercurrent $I(\delta\varphi)$ as function of the altermagnet length L for the junctions in Fig. 1, using different widths W. (a) Straight junction. (b) Diagonal junction. The parameter set is the same as in Fig. 2(a).

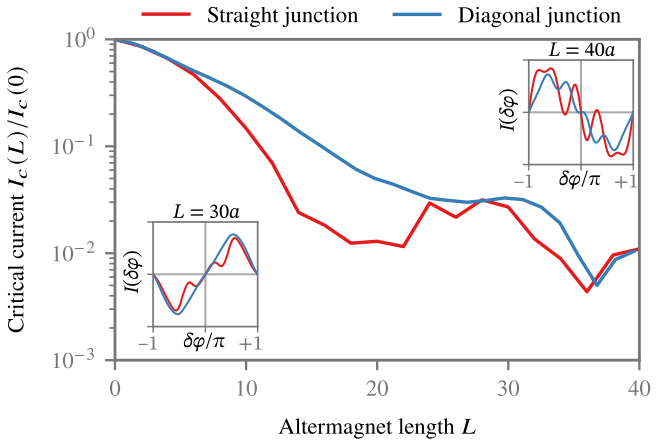

FIG. 4. Critical current I_c vs altermagnet length L for $m = 0.05t$ and $T = 0.05T_c$ [cf. Fig. 2(a)]. The insets show the current-phase relations for the indicated lengths, clearly demonstrating the sign reversal due to the 0-π transition.

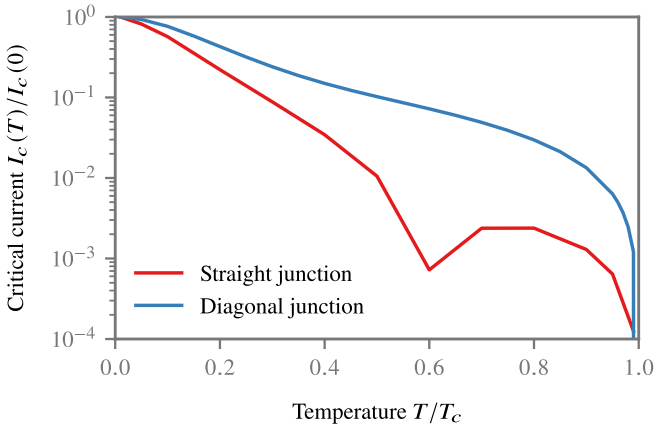

FIG. 5. Critical current I_c vs temperature T for $m = 0.15t$ and $L = 12a$ [cf. Fig. 2(b)].

oscillation for $L \approx 35a$, which for the diagonal junction is the first 0-π oscillation.

Figure 5 shows the critical current I_c vs temperature T, which is one experimental signature of 0-π transitions in Josephson junctions [17]. For these calculations, we picked an altermagnet length $L = 12a$ which according to Fig. 2(b) is close to a 0-π transition for straight but not diagonal junctions. For the straight junction, we find a nonmonotonic critical current that dips sharply at $T = 0.6T_c$. For both $T = 0.5T_c$ and $T = 0.7T_c$, the current-phase relation is completely dominated by the first harmonic I_1. However, it changes sign between these two points, so the dip is a signature of a 0-π transition as a function of temperature. This is in contrast to the diagonal junction, where we find no 0-π transition for these parameters. The supercurrent flow anisotropy can be tested within a single sample by depositing two superconducting electrode pairs, well separated from each other, on the same altermagnetic sample. Positioning the electrode pairs so that they are rotated 45° relative to each other, a current passed through one such pair would depend differently on temperature compared to current passed through the other pair, since each pair probes the diagonal and straight junction setup, respectively.

In summary, we have demonstrated that the Josephson effect through altermagnets, despite a vanishing net magnetization, displays 0-π oscillations in the Josephson effect. The decay and oscillation period strongly depends on the crystallographic orientation of the altermagnet relative the superconductors. The Josephson effect can be used both to distinguish the altermagnet from conventional (anti)ferromagnetism and additionally offers a way to change the supercurrent via flow direction anisotropy.

We thank A. Qaiumzadeh, L. Smejkal, J. Sinova, and T. Jungwirth for helpful comments. This work was supported by the Research Council of Norway through Grant No. 323766 and its Centres of Excellence funding scheme Grant No. 262633 "QuSpin." The simulations were performed on resources provided by Sigma2, project nn9577k —the National Infrastructure for High Performance Computing and Data Storage in Norway.

[1] A. Hirohata, K. Yamada, Y. Nakatani, I.-L. Prejbeanu, B. Dieny, P. Pirro, and B. Hillebrands, J. Magn. Magn. Mater. **509**, 166711 (2020).
[2] K.-H. Ahn, A. Hariki, K.-W. Lee, and J. Kunes, Phys. Rev. B **99**, 184432 (2019).
[3] S. Hayami, Y. Yanagi, and H. Kusunose, J. Phys. Soc. Jpn. **88**, 123702 (2019).
[4] L.-D. Yuan, Z. Wang, J.-W. Luo, E. I. Rashba, and A. Zunger, Phys. Rev. B **102**, 014422 (2020).
[5] L. Šmejkal, R. González-Hernández, T. Jungwirth, and J. Sinova, Sci. Adv. **6**, 8809 (2020).
[6] S. I. Pekar and E. I. Rashba, Zh. Eksp. Teor. Fiz. **47**, 1927 (1964).
[7] L. Šmejkal, J. Sinova, and T. Jungwirth, Phys. Rev. X **12**, 040501 (2022).
[8] L. Šmejkal, J. Sinova, and T. Jungwirth, Phys. Rev. X **12**, 031042 (2022).
[9] S. Bhowal and N. A. Spaldin, arXiv:2212.03756.
[10] H. Reichlova *et al.*, arXiv:2012.15651.
[11] S. Lopez-Moreno, A. H. Romero, J. Mejia-Lopez, and A. Muñoz, Phys. Chem. Chem. Phys. **18**, 33250 (2016).
[12] L.-D. Yuan, Z. Wang, J.-W. Luo, and A. Zunger, Phys. Rev. Mater. **5**, 014409 (2021).
[13] S. Hayami, Y. Yanagi, and H. Kusunose, Phys. Rev. B **102**, 144441 (2020).
[14] J. Clarke, Proc. R. Soc. A **308**, 447 (1969).
[15] Y. Oda and H. Nagano, Solid State Commun. **35**, 631 (1980).
[16] A. I. Buzdin, Rev. Mod. Phys. **77**, 935 (2005).
[17] V. V. Ryazanov, V. A. Oboznov, A. Yu. Rusanov, A. V. Veretennikov, A. A. Golubov, and J. Aarts, Phys. Rev. Lett. **86**, 2427 (2001).
[18] L. Ioffe, V. Geskenbein, M. Feigelman, A. Fauchere, and G. Blatter, Nature (London) **398**, 679 (1999).
[19] A. K. Feofanov, V. A. Oboznov, V. V. Bol'ginov, J. Lisenfeld, S. Poletto, V. V. Ryazanov, A. N. Rossolenko, M. Khabipov, D. Balashov, A. B. Zorin, P. N. Dmitriev, V. P. Koshelets, and A. V. Ustinov, Nat. Phys. **6**, 593 (2010).
[20] V. Geshkenbein and A. Larkin, Pis'ma Zh. Eksp. Teor. Fiz. **43**, 306 (1986).
[21] A. Millis, D. Rainer, and J. A. Sauls, Phys. Rev. B **38**, 4504 (1988).
[22] D. B. Szombati, S. Nadj-Perge, D. Car, S. R. Plissard, E. P. A. M. Bakkers, and L. P. Kouwenhoven, Nat. Phys. **12**, 568 (2016).
[23] B. M. Andersen, I. V. Bobkova, P. J. Hirschfeld, and Yu. S. arash, Phys. Rev. Lett. **96**, 117005 (2006).
[24] L. Bulaevskii, R. Eneias, and A. Ferraz, Phys. Rev. B **95**, 104513 (2017).
[25] J.-X. Zhu, Bogoliubov-de Gennes Method and Its Applications (Springer International Publishing, 2016).
[26] P. G. de Gennes, Superconductivity of Metals and Alloys (CRC Press, 1966).

[27] See Supplemental Material at http://link.aps.org/supplemental/10.1103/PhysRevLett.131.076003 for motivation of the tight-binding Hamiltonian and simulation results for ferromagnetic junctions.
[28] A. Weiße, G. Wellein, A. Alvermann, and H. Fehske, Rev. Mod. Phys. **78**, 275 (2006).
[29] L. Covaci, F. M. Peeters, and M. Berciu, Phys. Rev. Lett. **105**, 167006 (2010).
[30] Y. Nagai, Y. Ota, and M. Machida, J. Phys. Soc. Jpn. **81**, 024710 (2012).
[31] S. Goedecker, Rev. Mod. Phys. **71**, 1085 (1999).
[32] A. L. Benfenati, Numerical solutions to non-linear inhomogeneous problems in superconductivity, Ph.D. thesis, KTH, 2022.
[33] V. A. Oboznov, V. V. Bol'ginov, A. K. Feofanov, V. V. Ryazanov, and A. I. Buzdin, Phys. Rev. Lett. **96**, 197003 (2006).
[34] Jerome Cayssol and Gilles Montambaux, Phys. Rev. B **71**, 012507 (2005).